

1 Cost-benefit analysis of coastal flood defence measures in the North 2 Adriatic Sea

3 Mattia Amadio¹, Arthur H. Essenfelder¹, Stefano Bagli², Sepehr Marzi¹, Paolo Mazzoli², Jaroslav Mysiak¹,
4 Stephen Roberts³

5 ¹ *Centro Euro-Mediterraneo sui Cambiamenti Climatici, Università Ca' Foscari Venezia, Italy*

6 ² *Gecosistema, Rimini, Italy*

7 ³ *The Australian National University, Canberra, Australia*

8 Abstract

9 The combined effect of sea level rise and land subsidence phenomena poses a major threat to coastal
10 settlements. Coastal flooding events are expected to grow in frequency and magnitude, increasing the
11 potential economic losses and costs of adaptation. In Italy, a large share of the population and economic
12 activities are located along the coast of the peninsula, although risk of inundation is not uniformly distributed.
13 The low-lying coastal plain of Northeast Italy is the most sensitive to relative sea level changes. Over the last
14 half a century, the entire north-eastern Italian coast has experienced a significant rise in relative sea level, the
15 main component of which was land subsidence. In the forthcoming decades, climate-induced sea level rise is
16 expected to become the first driver of coastal inundation hazard. We propose an assessment of flood hazard
17 and risk linked with extreme sea level scenarios, both under historical conditions and sea level rise projections
18 at 2050 and 2100. We run a hydrodynamic inundation model on two pilot sites located in the North Adriatic
19 Sea along the Emilia-Romagna coast: Rimini and Cesenatico. Here, we compare alternative risk scenarios
20 accounting for the effect of planned and hypothetical seaside renovation projects against the historical
21 baseline. We apply a flood damage model developed for Italy to estimate the potential economic damage
22 linked to flood scenarios and we calculate the change in expected annual damage according to changes in the
23 relative sea level. Finally, damage reduction benefits are evaluated by means of cost-benefit analysis. Results
24 suggest an overall profitability of the investigated projects over time, with increasing benefits due to increased
25 probability of intense flooding in the next future.

26 **Key-words:** coastal inundation Italy extreme sea level rise

27 **Abbreviations:** MSL (Mean Sea Level); TWL (Total Water Level); ESL (Extreme Sea Level); SLR (Sea Level
28 Rise); VLM (Vertical Land Movements); DTM (Digital Terrain Model); EAD (Expected Annual Damage)

29 1. Introduction

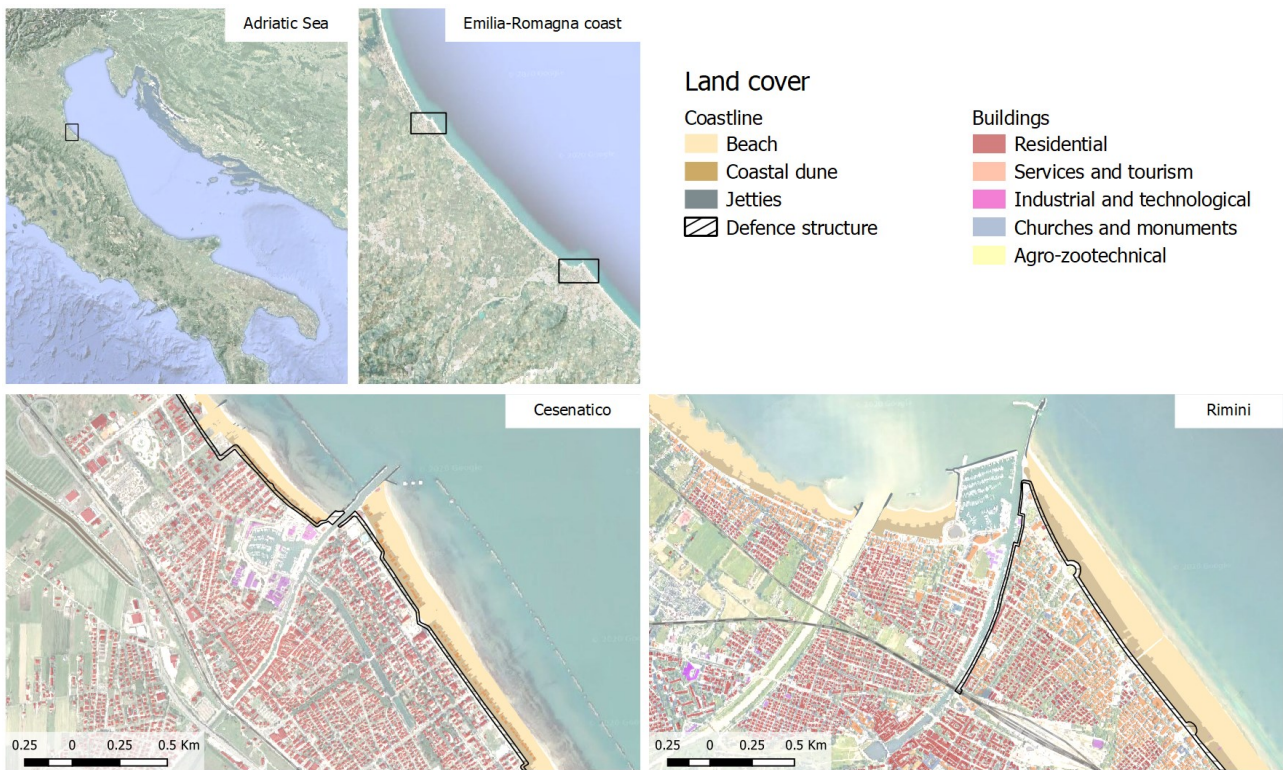
30 Globally, more than 700 million people live in low-lying coastal areas (McGranahan et al. 2007), and about
31 13% of them are exposed to a 100-year return period flood event (Muis et al. 2016). On average, one million
32 people located in coastal areas are flooded every year (Hinkel et al. 2014). Coastal flood risk shows an
33 increasing trend in many places due to socio-economic growth (Bouwer 2011; Jongman et al. 2012b) and land
34 subsidence (Syvitski et al. 2009; Nicholls and Cazenave 2010), but in the near future sea level rise (SLR) will
35 likely be the most important driver of increased coastal inundation risk (Hallegatte et al. 2013; Hinkel et al.
36 2014). Evidences show that global sea level has risen at faster rates in the past two centuries compared to the
37 millennial trend (Kemp et al. 2011; Church and White 2011), topping 3.2 mm per year in the last decades
38 mainly due to ocean thermal expansion and glacier melting processes (Mitchum et al. 2010; Meyssignac and
39 Cazenave 2012). According to the IPCC projections, it is very likely that, by the end of the 21st century, the
40 SLR rate will exceed that observed in the period 1971-2010 for all Representative Concentration Pathway (RCP)
41 scenarios (IPCC 2019); yet the local sea level can have a strong regional variability, with some places

42 experiencing significant deviations from the global mean change (Stocker et al. 2013). This is particularly
43 worrisome in regions where changes in the mean sea level (MSL) are more pronounced, considering that even
44 small increases of MSL can drastically change the frequency of extreme sea level (ESL) events, leading up to
45 situations where a 100-year event may occur several times per year by 2100 (Carbognin et al. 2009, 2010;
46 Vousdoukas et al. 2017, 2018; Kirezci et al. 2020). Changes in the frequency of extreme events are likely to
47 make existing coastal protection inadequate in many places, causing a large part of the European coasts to be
48 exposed to flood hazard. Under these premises, coastal floods threaten to trigger devastating impacts on
49 human settlements and activities (Lowe et al. 2001; McInnes et al. 2003; Vousdoukas et al. 2017). In this context,
50 successful coastal risk mitigation and adaptation actions require accurate and detailed information about the
51 characterisation of coastal flood hazard and the performance of alternative coastal defence options. Cost-
52 benefit analysis (CBA) is widely used to evaluate the economic desirability of a disaster risk reduction (DRR)
53 project (Jonkman et al. 2004; Mechler 2016; Price 2018). CBA helps decision-makers in evaluating the efficacy
54 of different adaptation options (Kind 2014; Bos and Zwaneveld 2017).

55 In this study, designed coastal renovation projects in the municipalities of Rimini and Cesenatico, in Italy, are
56 compared against the baseline scenario in terms of net economic benefits under changing climate conditions.
57 First, we employ the 2D-hydrodynamic ANUGA model (Roberts et al. 2015) for simulating coastal inundation
58 scenarios associated with ESL projections over the two pilot areas located along the Emilia-Romagna coast
59 (North Adriatic Sea). Flood hazard maps are produced for current conditions (2020) and future conditions
60 (2050 and 2100) by combining the local data from historical ESL events with the estimates of relative mean sea
61 level (RMSL) change for those locations. RMSL change accounts for both the eustatic global rise and the locally-
62 measured land vertical movement effect. Each inundation scenario simulated by the model is translated in
63 terms of direct economic impacts over residential areas using a locally-calibrated damage model. The
64 combination of different risk scenarios in a CBA framework allows to evaluate the economic benefits brought
65 by the project implementation in terms of avoided direct flood losses up to the end of the century.

66 **2. Area of study**

67 Located in the central Mediterranean Sea, the Italian peninsula has more than 8,300 km of coasts, hosting
68 around 18% of the country population, numerous towns and cities, industrial plants, commercial harbours
69 and touristic activities, as well as cultural and natural heritage sites. Existing country-scale estimates of SLR
70 up to the end of this century helps to identify the most critically exposed coastal areas of Italy (Lambeck et al.
71 2011; Bonaduce et al. 2016; Antonioli et al. 2017; Marsico et al. 2017). About 40% of the coastal perimeter consist
72 of a flat coastal profile (ISPRA 2012), potentially more vulnerable to the impacts of ESL events. The North
73 Adriatic coastal plain is acknowledged to be the largest and most vulnerable location to extreme coastal events
74 due to the shape, morphology and low bathymetry of the Adriatic sea basin, which cause water level to
75 increase relatively fast during coastal storms (Carbognin et al. 2010; Ciavola and Coco 2017; Perini et al. 2017).
76 The ESL here is driven mainly by astronomical tide, ranging about one meter in the northernmost sector; and
77 meteorological forcing, such as low pressure, seiches and prolonged rotational wind systems, which are the
78 main trigger of storm surge in the Adriatic basin (Vousdoukas et al. 2017; Umgiesser et al. 2020). In addition
79 to that, all the coastal profile of the Padan plain shows relatively fast subsiding rates, partially due to natural
80 phenomena, but in large part linked to human activities (Carbognin et al. 2009; Perini et al. 2017; Meli et al.
81 2021). As a contributing factor to coastal flood risk, the intensification of urbanization has led to increased
82 exposure along the Adriatic coast during the last 50 years, with many regions building over half of the
83 available land within 300 meters from the shoreline (ISPRA 2012). This study focuses on two pilot sites located
84 along the Adriatic coast of Emilia-Romagna, shown in figure 1: Cesenatico and Rimini.



85
 86 **Figure 1.** Pilot areas locations along the Emilia-Romagna coast: Cesenatico and Rimini. The coastal defence
 87 structure assessed in this study are shown in black. Buildings' footprint data from Regional Environmental
 88 Agency (ARPA) 2020. Basemap © Google Maps 2020.

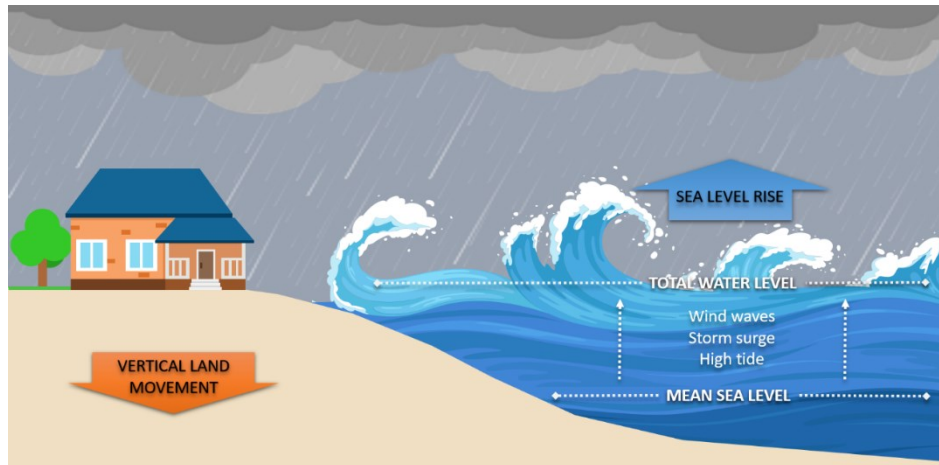
89 The number of ESL events reported to cause impacts along the Emilia-Romagna coast shows a steady increase
 90 since the second half of the past century (Perini et al. 2011), which is in part explained by to the socio-economic
 91 development of the coast exposing increasing asset to flood risk. The landscape along the 130 km regional
 92 coastline is almost flat, the only relief being old beach ridges, artificial embankments and a small number of
 93 dunes. The coastal perimeter is delineated by a wide sandy beach that is generally protected by offshore
 94 breakwaters, groins and jetties. The land elevation is often close to (or even below) the MSL, while the coastal
 95 corridor is heavily urbanised. Cesenatico has about 26,000 residents, while Rimini has 150,000. These port
 96 towns have a strong touristic vocation, hosting large beach resort and bathing facilities along the beach and
 97 hundreds of hotels and rental housing located just behind the seaside. Both towns have been affected by
 98 coastal storms resulting in flooding of buildings and activities, beach erosion and regression of the coastline.
 99 The most recent inundation events were observed in March 2010, November 2012 and February 2015. The 2015
 100 event was one of the most severe ever recorded, with ESL values corresponding to a probability of once in 100
 101 years. It caused severe damages along the whole regional coast and, in some locations, required the evacuation
 102 of people from their houses; many buildings and roads were covered by sand brought by the flood wave;
 103 touristic infrastructures near the shore were seriously damaged, and some port channels overflowed the
 104 surrounding areas. The economic impact was estimated topping 7.5 M Eur (Perini et al. 2015).

105 3. Methodology

106 3.1 Components of the analysis

107 Coastal inundation phenomena are caused by an increase of total water level (TWL), most often associated to
 108 extreme sea level (ESL) events, which are generated by a combination of high astronomical tide and
 109 meteorological drivers such as storm surge and wind waves (figure 2). Estimates of ESL are obtained for the

110 North Adriatic up to year 2100 by combining reference hazard scenarios derived from historical records with
 111 regionalised projections of SLR (Vousdoukas et al. 2017) and local vertical land movements (VLM) rates
 112 (Carbognin et al. 2009; Perini et al. 2017). Four ESL frequency scenarios, namely once in 1, 10, 100- and 250-
 113 years, are considered. The hydrodynamic model ANUGA is applied to simulate the inundation of land areas
 114 during ESL accounting for individual components (storm surge, tides and waves). Land morphology and
 115 exposure of coastal settlements are described by high-resolution DTM and bathymetry, in combination with
 116 land use and buildings footprints. The effect of hazard mitigation structures (both designed and under
 117 construction) are explicitly accounted in the “defended” simulation scenario, in contrast to the baseline
 118 scenario, where only existing defence structures (groins, jetties, breakwaters and sand dunes) are accounted.



119
 120 **Figure 2.** Components of the analysis for extreme sea level events: total water level is the sum of maximum
 121 tide, storm surge and wind waves over mean sea level. Vertical land movement and eustatic sea level rise
 122 affects the mean sea level on the long run.

123 3.2 Vertical Land Movement

124 Vertical land movements result from a combination of slow geological processes such as tectonic activity and
 125 glacial isostatic adjustment (Peltier 2004; Peltier et al. 2015), and medium-term phenomena, such as sediment
 126 loading and soil compaction (Carminati and Martinelli 2002; Lambeck and Purcell 2005). The latter can greatly
 127 oversize geological processes at local scale (Wöppelmann and Marcos 2012); in particular, faster subsidence
 128 occurs in presence of intense anthropogenic activities such as water withdrawal and natural gas extraction
 129 (Teatini et al. 2006; Polcari et al. 2018). Most of the peninsula shows a slow subsiding trend, although with
 130 some local variability. An estimate of VLM rates due to tectonic activity has been derived from studies
 131 conducted in Italy (Lambeck et al. 2011; Antonioli et al. 2017; Marsico et al. 2017; Solari et al. 2018). The North
 132 Adriatic coastal plain shows the most intense long-term geological subsidence rates (about 1 mm per year),
 133 increasing North to South. Yet in the last decades these rates were often greatly exceeded by ground
 134 compaction rates observed by multi-temporal SAR Interferometry (Gambolati et al. 1998; Antonioli et al. 2017;
 135 Polcari et al. 2018; Solari et al. 2018). Observed subsidence is about one order of magnitude faster where the
 136 aquifer system has been extensively exploited for agricultural, industrial and civil use since the post-war
 137 industrial boom. From the 1970s, however, with the halt of groundwater withdrawals, anthropogenic
 138 subsidence has been strongly reduced or stopped, but many of the induced effects still remain (Carbognin et
 139 al. 2009). Geodetic surveys carried out from 1953 to 2003 along the Ravenna coast provide evidence of a
 140 cumulative land subsidence exceeding 1 m at some sites due to gas extraction activities. Average subsidence
 141 rates observed for 2006-2011 along the Emilia-Romagna coast are around 5 mm/yr, exceeding 10 mm/yr in the
 142 back shore of the Cesenatico and Rimini areas and topping 20-50 mm/yr in Ravenna (Carbognin et al. 2009;
 143 Perini et al. 2017). Based on these current rates, we assume an average fixed annual VLM of 5 mm in both

144 Cesenatico and Rimini up to the end of the century. This remarkable difference between natural VLM rates
145 and observations would produce a dramatic effect on the estimated SLR scenarios: at present rates, Rimini
146 would see an increase of MSL by 0.15 m in 2050 and more than 0.4 m in 2100 independently from eustatic SLR.
147 Since these rates are connected with human activity, it is not possible to foresee exactly how they will change
148 in the long term.

149 3.3 Sea Level Rise

150 The long availability of tide gauge data along the N Adriatic coast allows to assess the changes in MSL during
151 the last century. Records from the gauge station of Marina di Ravenna show an eustatic rise of 1.2 mm per
152 year from 1890 to 2007 (Meli et al. 2021), in good agreement with the eustatic rise measured at other stations
153 in the Mediterranean Sea (Tsimplis and Rixen 2002; Carbognin et al. 2009). The projections of future MSL
154 account for sea thermal expansions from four global circulation models, estimated contributions from ice-
155 sheets and glaciers (Hinkel et al. 2014) and long-term subsidence projections (Peltier 2004). The ensemble mean
156 is chosen to represent each RCP for different time slices. The increase in the central Mediterranean basin is
157 projected to be approximately 0.2 m by 2050 and between 0.5 and 0.7 m by 2100, compared to historical mean
158 (1970-2004) (Vousdoukas et al. 2017). As agreed with stakeholders, our analysis considers the intermediate
159 emission scenario RCP 4.5, projecting an increase in MSL of 0.53 m at 2100. It must be noted that these
160 projections, although downscaled for the Adriatic basin, do not account for the peculiar continental
161 characteristics of the shallow northern Adriatic sector, where the hydrodynamics and oceanographic
162 parameters partially depend on the freshwater inflow (Zanchettin et al. 2007).

163 3.4 Tides and meteorological forcing

164 Storm surge and wind waves represent the largest contribution to TWL during an ESL event. An estimation
165 of these components is obtained for the pilot sites from the analysis of tide gauge and buoy records, and from
166 the description of historical extreme events presented in local studies (Perini et al. 2011, 2012, 2017; Masina et
167 al. 2015; Armaroli and Duo 2018). This area is microtidal: the mean neap tidal range is 30–40 cm, and the mean
168 spring tidal range is 80–90 cm. Most storms have a duration of less than 24 h and a maximum significant wave
169 height of about 2.5 m. During extreme cyclonic events, the sequence of SE wind (*Sirocco*) piling the water North
170 and E-NE wind (*Bora*) pushing waves towards the coast can generate severe inundation events, with
171 significant wave height ranging 3.3 – 4.7 m and exceptionally exceeding 5.5 m (Armaroli et al. 2012). Fifty
172 significant events have been recorded from 1946 to 2010 on the ER coast, with half of them causing severe
173 impacts along the whole coast and 10 of them being associated with important flooding events (Perini et al.
174 2017). The most severe events are found when strong winds blow during exceptional tide peaks, most often
175 happening in late autumn and winter. The event of November 1966 represents the highest ESL on records,
176 causing significant impacts along the regional coast: the recorded water level was 1.20 m above MSL, and
177 wave heights offshore were estimated around 6–7 m (Perini et al. 2011; Garnier et al. 2018). The whole coastline
178 suffered from erosion and inundation, especially in the province of Rimini. Atmospheric forcing shown
179 significant variability for the period 1960 onwards (Tsimplis et al. 2012), but there is no strong evidence
180 supporting a significant change in trend for the next future (Lionello 2012; Lionello et al. 2020; Zanchettin et
181 al. 2020). Thus, we assume the frequency and intensity of meteorological events to remain the same up to 2100.

182 3.5 Terrain morphology and coastal defence structures

183 Reliable bathymetries and topography are required in order to run the hydrodynamic modelling at the local
184 scale. Bathymetric data for the Mediterranean Sea were obtained from the European Marine Observation and
185 Data Network (EMODnet) at 100 m resolution. The description of terrain morphology comes from the official

186 high-resolution LIDAR DTM (MATTM, 2019). First, we combined the coastal dataset (2 m resolution and
187 vertical accuracy of ± 0.2 m), and the inland dataset (1 m resolution and vertical accuracy ± 0.1 m) into one
188 seamless layer. Then, the DTM is supplemented with geometries of existing coastal protection elements such
189 as jetties, groins and breakwaters obtained from the digital Regional Technical Map. In Rimini, the Parco del
190 Mare is an urban renovation project which aims to improve the seafront promenade: the existing road and
191 parking lots are converted into an urban green infrastructure consisting of a concrete barrier covered by
192 vegetated sandy dunes with walking paths. This project also acts as a coastal defence system during extreme
193 sea level events. The barrier rises 2.8 meters along the southern section of the town, south of the marina; no
194 barrier is planned on the northern coastal perimeter. The Parco del Mare project, currently under construction,
195 has been taken in account in the evaluation of the “defended” scenarios by merging the barrier into the existing
196 DTM (figure 3).



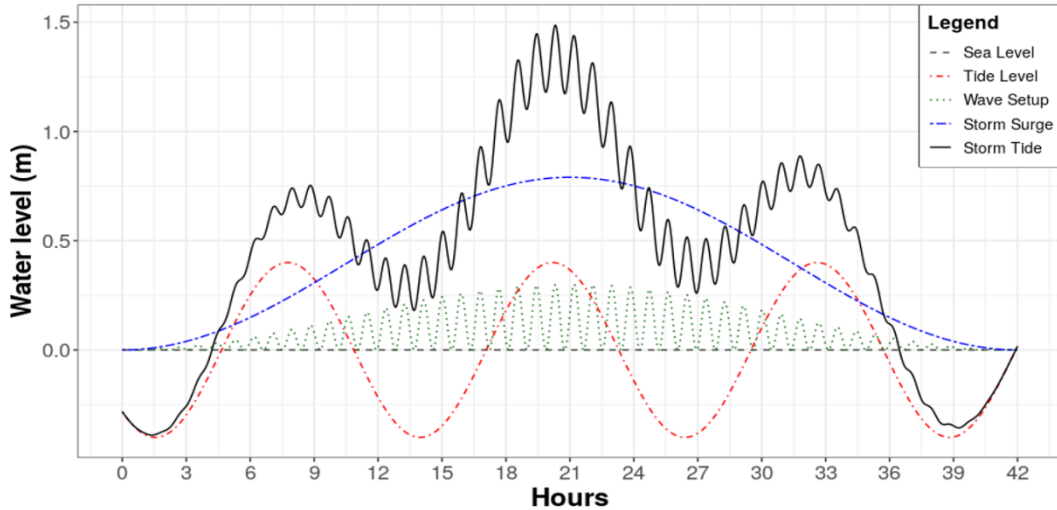
197
198 **Figure 3.** Prototype design of Parco del Mare project in Rimini. Adapted from JDS Architects.

199 In Cesenatico, the existing defence structures include a moving barriers system (*Porte Vinciane*) located on the
200 port channel, coupled with a dewatering pump which discharge the meteoric waters in the sea. The barriers
201 close automatically if the TWL surpasses 1 meter over the mean, preventing floods in the historical centre up
202 to ESL of 2.2 meters. Additional defence structures include the winter dunes, which consist of a 2.2 meter-tall
203 intermittent, non-reinforced sand barrier. In the defended scenario, we envisage a coastal defence structure
204 similar to Parco del Mare in Rimini, spanning both North and South of the port channel with a total length of
205 7.8 km. A proper setup of the inundation model required to first perform some manual editing of the DTM
206 using additional reference data (i.e. on-site observations or aerial photography) in order to produce an
207 elevation model that realistically represent the land morphology and associated water dynamics (e.g. removal
208 of non-existent sink holes). Bridges and tunnels are the most critical elements that required DTM correction in
209 order to avoid misrepresentations of the water flow routing.

210 3.6 Inundation modelling

211 At the local scale, hydrodynamic models represent an efficient compromise between hydrostatic and hydraulic
212 models, being able to perform realistic simulations of inundation phenomena and to obtain detailed
213 information about the hazard features, while requiring a relatively fast setup and reasonable computational
214 effort. In this study we use ANUGA, a 2D hydrodynamic model originally developed to simulate tsunami
215 events, which is also suitable for the simulation of hydrologic phenomena such as riverine peak flows and
216 storm surges (Roberts 2020). Being a 2D hydrodynamic model, ANUGA does not resolve vertical convection
217 and consequently not breaking waves or 3D turbulence (e.g. vorticity), thus not considering the swash
218 component of wave runup. The fluid dynamics in ANUGA is based on a finite-volume method for solving the
219 shallow water wave equations, thus being based on continuity and simplified momentum equation. The
220 model computes the total water level, the water depth, and the horizontal momentum on an irregular

221 triangular grid based on the provided forcing conditions. ANUGA includes also an operator module that
 222 simulates the removal of sand associated with over-topping of a sand dune by sea waves, which is applied to
 223 explore scenarios where a sand dune barrier provides protection for the land behind. The operator simulates
 224 the erosion, collapse, fluidisation and removal of sand from the dune system (Kain et al. 2020); the dune
 225 erosion mechanism relies on a relationship based on Froehlich (2002). This option is enabled only in the
 226 undefended scenario for Cesenatico, where non-reinforced sand dunes are prone to erosion.



227
 228 **Figure 4.** Total Water Level (black) as a sum of tide (red), storm surge (blue) and wave setup (green) for ESL
 229 scenario 1 in 10 years.

230 In our application, we estimate the TWL on the coastland at every timestep as the sum of extreme values for
 231 storm surge level (SS), wave setup (Ws), and max tide ($Tmax$), as shown in figure 4. The maximum tidal
 232 excursion is 0.8 m, while wave height can range from 3 to almost 6 m during strong wind events, translated
 233 into a wave setup near the shore ranging from 0.22 to 0.65 m. Additional details are wave period (Wp , in
 234 seconds) and event duration ($Time$, in hours), required to estimate the maximum extent of inland water
 235 propagation. Wave direction is oriented perpendicular to the coast. Storm surge is set to peak in the mid of
 236 the event, producing the maximum TWL value for the event. The most exceptional ESL events can last up to
 237 3 days. Table 1 summarizes the ESL components according to the four probability scenarios identified from
 238 local historical records (Perini et al. 2017). The probability of occurrence is expressed in terms of return period
 239 (RP), which is the estimated average time interval between events of similar intensity. The output of the
 240 simulation consists of maps representing flood extent, water depth and momentum at every time step (1
 241 second), projected on the high-resolution DTM grid.

242 **Table 1.** components of TWL during an ESL event under historical conditions and projected conditions (2050
 243 and 2100), accounting for both eustatic SLR (RCP4.5) and average VLM rate.

RP (years)	Extreme event features				Historical TWL (m)	2050			2100		
	SS (m)	$Tmax$ (m)	Ws (m)	$Time$ (h)		SLR (m)	VLM (m)	TWL (m)	SLR (m)	VLM (m)	TWL (m)
1	0.60	0.40	0.22	32	1.2	0.14	0.19	1.55	0.53	0.44	2.2
10	0.79	0.40	0.30	42	1.5	0.14	0.19	1.82	0.53	0.44	2.5
100	1.02	0.40	0.39	55	1.8	0.14	0.19	2.14	0.53	0.44	2.8
250	1.40	0.45	0.65	75	2.5	0.14	0.19	2.83	0.53	0.44	3.5

244 3.7 Risk modelling and Expected Annual Damage

245 Direct damage to physical asset is estimated using a customary flood risk assessment approach originally
246 developed for fluvial inundation, which is adapted to coastal flooding assuming that the dynamic of impact
247 from long-setting floods depends on the same factors, namely: 1) hazard magnitude, and 2) size and value of
248 exposed asset. Indirect economic losses due to secondary effects of damage (e.g. business interruption) are
249 excluded from the computation. Hazard magnitude can be defined by a range of variables, but the most
250 important predictors of damage are water depth and the extension of the flood event (Jongman et al. 2012a;
251 Huizinga et al. 2017). Land cover definitions and buildings footprints help to estimate the exposed capital
252 including residential buildings, commercial and industrial activities, infrastructures, historical and natural
253 sites. The characterization of exposed asset is built from a variety of sources, starting from land use and
254 buildings footprints obtained from the Regional Environmental Agencies geodatabases and the Open Street
255 Map database (Geofabrik GmbH 2018). Additional indicators about buildings characteristics are obtained
256 from the database of the official Italian Census of 2011 (ISTAT 2011), while mean construction and restoration
257 costs per building types are obtained from cadastral estimates (CRESME 2014). The asset representation is
258 static, thus not accounting for changes in land use nor population density, while allowing for the direct
259 comparison of hazard mitigation options' results. A depth-damage function was previously validated on
260 empirical records (Amadio et al. 2019) and then applied in order to translate each hazard scenario into an
261 estimate of economic risk, measured as a share of total exposed value. The damage function applies only to
262 residential and mixed-residential buildings, the area of which represents about 93% of total exposed footprints;
263 other types (such as harbour infrastructures, industrial, commercial, historical monuments and natural sites)
264 are excluded from risk computation. Abandoned or under-construction buildings are also excluded from the
265 analysis. To avoid overcounting of marginally-affected buildings, we set two threshold conditions for damage
266 calculation: flood extent must be greater than or equal to 10 m², and maximum water depth greater than or
267 equal to 10 cm. The damage/probability scenarios are combined together as Expected Annual Damage (EAD).
268 EAD is the damage that would occur in any given year if damages from all flood probabilities were spread
269 out evenly over time; mathematically, EAD is the integration of the flood risk density curve over all
270 probabilities (Olsen et al. 2015), as in equation 1.

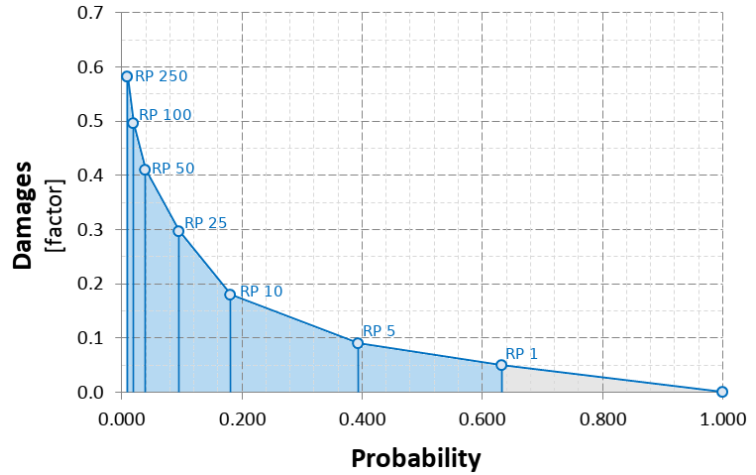
$$EAD = \int_0^1 D(p) dp \quad (1)$$

271 The integration of the curve can be solved either analytically or numerically, depending on the complexity of
272 the damage function $D(p)$. Several different methods for numerical integration exist; we use an approach
273 where EAD is the sum of the product of the fractions of exceedance probabilities by their corresponding
274 damages (figure 5). We calculate $D(p)$, which is the damage that occurs at the event with probability p , by
275 using the depth-damage function for each hazard scenario. The exceedance probability of each event (p) is
276 calculated based on exponential function as shown in equation 2.

$$p = 1 - e^{\left(\frac{-1}{RP}\right)} \quad (2)$$

277 Events with a high probability of occurrence and low intensity (below RP 1 year) are not simulated, as they
278 are assumed to not cause significant damage. This is consistent with the historical observations for the case
279 study area, although this assumption could change with increasing MSL.

Figure 5. Schematic representation of the numerical integration of the damage function $D(p)$ with respect to the exponential probability of the hazard events. Events with a probability of occurrence higher than once in a year are expected to not cause damage (grey area).



280 3.8 Cost-Benefit Analysis

281 A CBA should include a complete assessment of the impacts brought by the implementation of the hazard
 282 mitigation option, i.e. direct and indirect, tangible and intangible impacts (Bos and Zwaneveld 2017). The
 283 project we are considering, however, has not been primarily designed for DRR purpose: instead, it is meant
 284 as an urban renovation project which aims to consolidate the touristic vocation of the area, to improve the
 285 quality of life and the urban environment (Comune di Rimini 2018). This implies some large indirect effects
 286 on the whole area, most of which are not strictly related to disaster risk management and, overall, very difficult
 287 to estimate ex-ante. Our evaluation focuses only on the benefits that are measurable in terms of direct flood
 288 losses reduction. Regarding the implementation costs, the CBA accounts for the initial investment required
 289 for setting up the adaptation measure, and operational costs through time. According to the “Parco del Mare”
 290 project funding documentation (Comune di Rimini 2019a, b, 2020, 2021a, b), the total cost of the project (to be
 291 completed during 2021) is 33.3 M Eur, corresponding to 5.55 M Eur per Km of length. No information is
 292 available about maintenance costs of the opera, but given the nature of the project (static defense with low
 293 structural fragility), we assume they will be rather small compared to the initial investment. Ordinary annual
 294 maintenance costs are accounted as 0.1% of the total cost of the project. The same costs are assumed for the
 295 hypothetical barrier in Cesenatico, resulting in an initial investment cost of 43.3 M. Costs and benefit occurring
 296 in the future periods need to be discounted, as people put higher value on the present (Rose et al., 2007). This
 297 is done by adjusting future costs and benefits using an annual discount rate (r). We chose a variable rate of $r =$
 298 3.5 for the first 50 years and $r = 3$ from 2050 onward (Lowe 2008). A sensitivity analysis of discount rate is
 299 included in Annex 1. The three main decision criteria used in CBA for project evaluation are the Net Present
 300 Value (NPV), the Benefit/Cost Ratio (BCR) and the payback period. The NPV is the sum of Expected Annual
 301 Benefits (B) up to the end of the time horizon, discounted, minus the total costs for the implementation of the
 302 defense measure, which takes into account initial investment plus discounted annual maintenance costs (C).
 303 In other words, the NPV of a project equals the present value of the net benefits ($NB_i = B_i - C_i$) over a period of
 304 time (Boardman et al. 2018), as in equation (3):

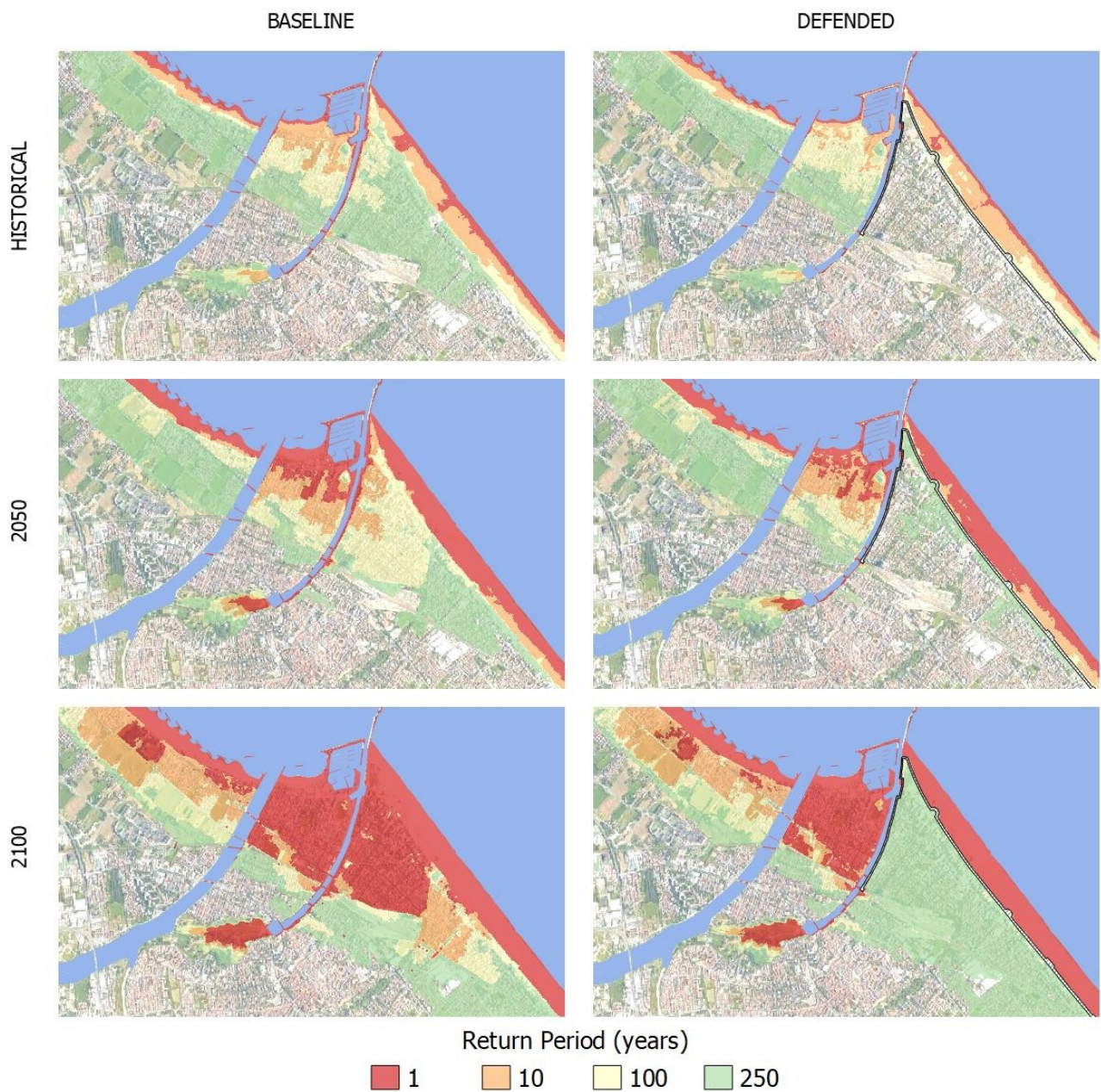
$$NPV = PV(B) - PV(C) = \sum_{t=0}^n \frac{NB_t}{(1+r)^t} \quad (3)$$

305 Positive NPV means that the project is economically profitable. The BCR is instead the ratio between the
 306 benefits and the costs; a BCR larger than 1 means that the benefits of the project exceed the costs on the long
 307 term and the project is considered profitable. The payback period is the number of years required for the
 308 discounted benefits to equal the total costs.

309 **4. Results**

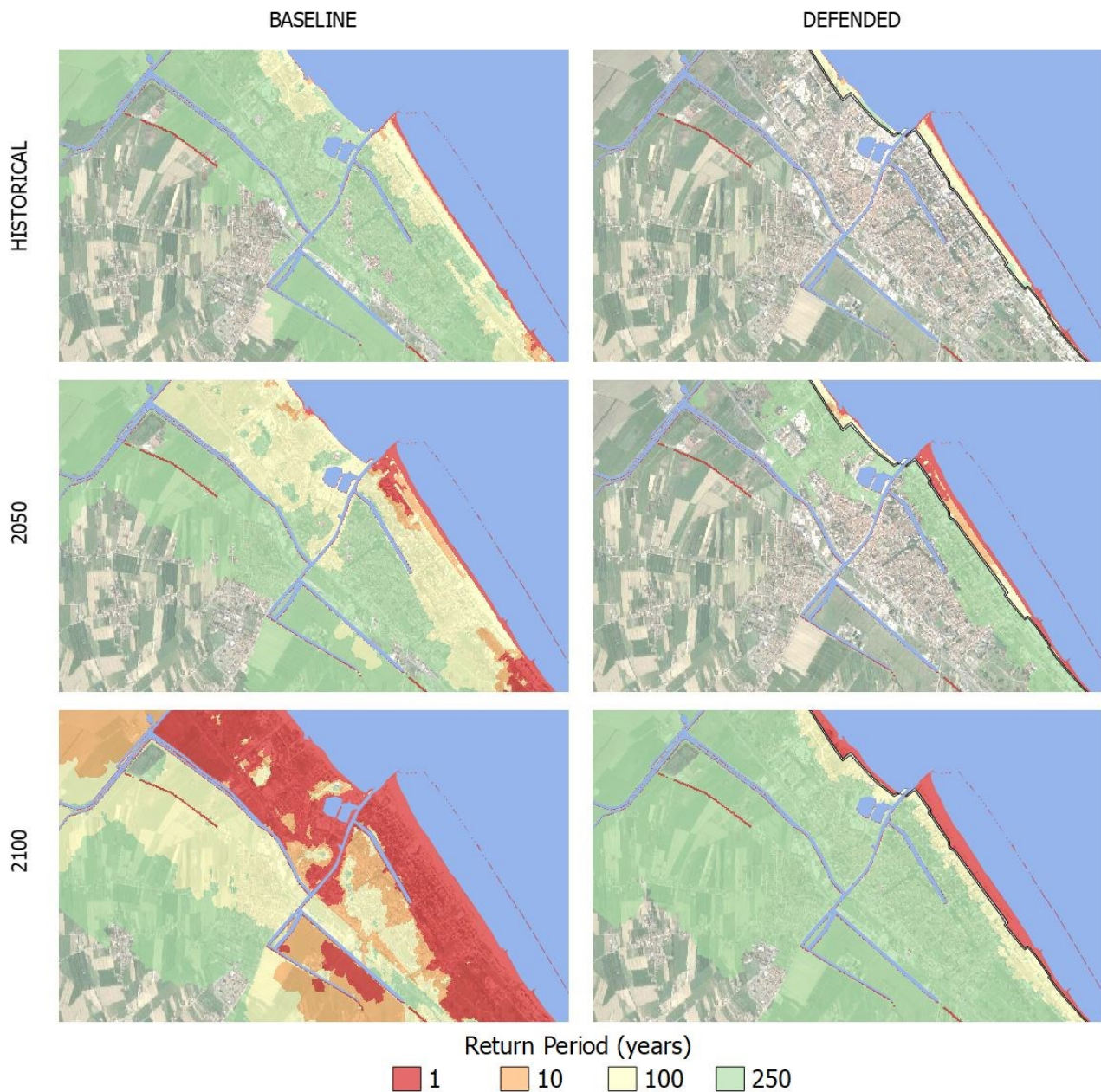
310 **4.1 Inundation scenarios**

311 Once the setup is completed, the hydrodynamic model performs relatively fast: each simulation is carried at
312 half speed compared to real time, requiring about 24 hours to simulate a 12 h event. Parallel simulations for
313 the same area can run on a multicore processor, improving the efficiency of the process. The output of the
314 hydrodynamic model consists of a set of inundation simulations that include several hazard intensity variables
315 in relation to flood extent: water depth, flow velocity, and duration of submersion. ESL scenarios are then
316 summarized into static maps, each one representing the maximum value reached by hazard intensity variables
317 at grid cell level (about 1 meter) during the whole simulated event. The flood extents corresponding to each
318 RP scenario are shown for Rimini (figure 6) and Cesenatico (figure 7).



319 **Figure 6.** Rimini, extent of land affected by flood according to frequency of occurrence of ESL event up to 2100
320 for the baseline [left] and the defended scenario [right]. Basemap © Google Maps 2020.
321

322 In Rimini, the Parco del Mare barrier produces benefits in terms of avoided damage in the south-eastern part
 323 of the town (high-density area) for ESL events with a return period of 100 years or less. The north-western part
 324 and the marina are outside of the defended area; these areas are therefore subject to a similar amount of
 325 flooding across scenarios. In all the simulations, the buildings located behind the marina are the firsts to be
 326 flooded. In fact, the new and the old port channels located on both sides of the marina represent a hazard
 327 hotspot: as shown in the maps, the failure of the eastern channel, which has a relatively low elevation, is likely
 328 to cause the water to flood the eastern part of the town, even during inundation events that would not surpass
 329 the beach. In the defended scenarios, where both the coastal and the canal barriers are enabled, the flood extent
 330 in the SE urban area becomes almost zero for ESL events with a probability of once in 100 years, even when
 331 accounting for SLR up to 2100. Under more exceptional ESL conditions (RP 250 in 2100), the barrier is
 332 surmounted, generating a flood extent similar to the baseline scenario for the same occurrence probability.

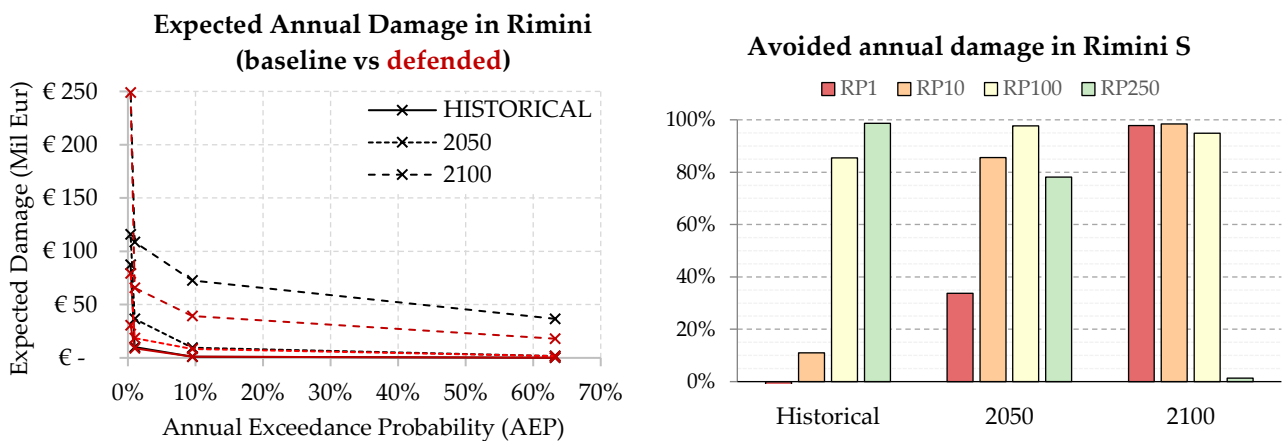


333
 334 **Figure 7.** Cesenatico, extent of land affected by flood according to frequency of occurrence of ESL event up to
 335 2100 for the baseline [left] and the defended scenario [right]. Basemap © Google Maps 2020.

336 In Cesenatico, a barrier designed similarly to Parco del Mare could provide significant reduction of flood
 337 extents under most hazard scenarios. Its effectiveness would be greater than in Rimini thanks to the
 338 complementary movable barrier system in use, which seals the port channel allowing to wall off the whole
 339 coastal perimeter, reducing the chance of water ingression in the urban area. In contrast, the erodible winter
 340 dune in the baseline defense scenario can only hold the heavy sea for shorter, less intense ESL events, and
 341 becomes ineffective with more exceptional, long-lasting events; at 2050 and 2100, the winter dune gets
 342 surmounted and dismantled by sea waves for scenario RP250 years (mid- and low-left maps).

343 4.2 Expected Annual Damage

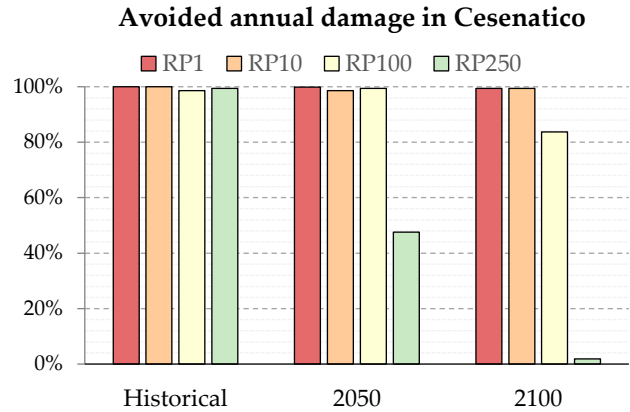
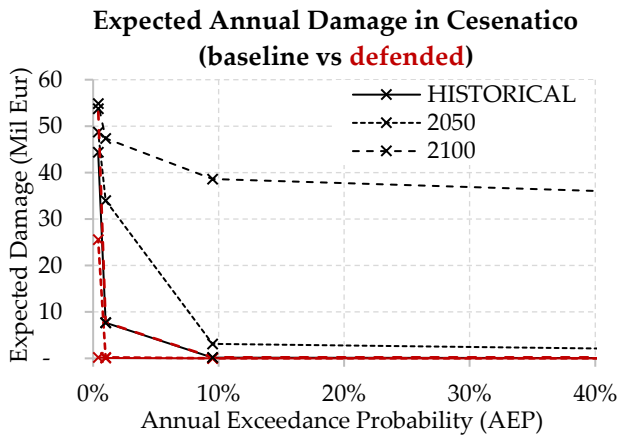
344 The Expected Annual Damage is calculated as a function of maximum exposed value and water depth. In
 345 Rimini, the EAD grows from around 65 thousand Eur under historical conditions to 2.8 million Eur in 2050
 346 and more than 32.3 million Eur in 2100. With less severe events (up to RP 100 years), the risk remains mostly
 347 confined around the marina area (outside the protection offered by the reinforced dune) producing an EAD
 348 below 10 thousand Eur; with more intense ESL scenarios (i.e. RP 250 years), the benefits of the dune barrier
 349 protecting the southern part of Rimini become more evident, avoiding about 65% of the EAD. The damage
 350 avoided in the defended area grows almost linearly with the increase of EAD under future projections of sea
 351 level rise: under the defended hypothesis, the EAD is reduced on average by 45% (figure 8, left). The project
 352 produces benefit up to ESL RP250 years in 2100, where a projected TWL of 3.5 meters would cause the
 353 surmounting of the barrier, reducing the benefits to almost zero (figure 8, right).



354

355 **Figure 8.** Rimini: Expected Annual Damage (EAD) according to undefended scenario up to 2100 [left]; EAD
 356 reduction in the South part of the town thanks to hazard mitigation offered by the coastal barrier [right].

357 In Cesenatico, the average EAD for the undefended scenario grows from around 270 thousand Eur under
 358 historical conditions, to 1.7 million Eur in 2050 and almost 26 million Eur in 2100. In our simulations, the
 359 designed defence structure (a static barrier with height of 2.8 m along 7.8 km of coast) is able to avoid most of
 360 the damage inflicted to residential buildings (figure 9, left). The measure becomes less efficient for the most
 361 extreme scenarios in 2050 and 2100, when the increase in TWL causes the surmounting of the barrier (figure
 362 9, right). This assessment does not account for the beach resorts and bathing facilities, which are located along
 363 the barrier or between the barrier and the sea, and thus are equally exposed in both the baseline and the
 364 defended scenario; they would likely represent an additional 7-25% of the baseline damage.

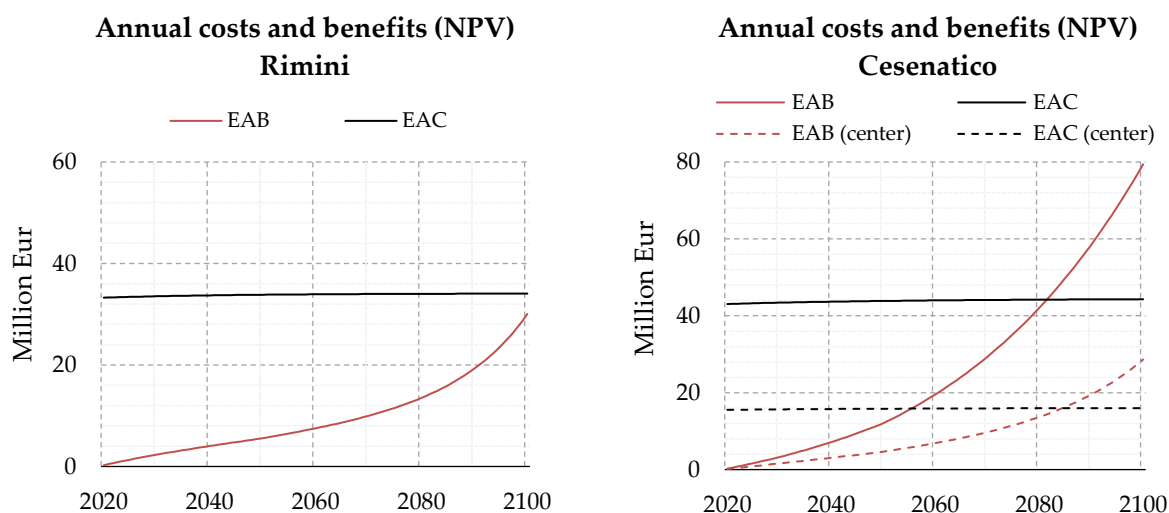


365
 366 **Figure 9.** Cesenatico: Expected Annual Damage (EAD) according to undefended scenario up to 2100 [left];
 367 EAD reduction thanks to hazard mitigation offered by the coastal barrier [right].

368 **4.3 Cost-Benefit Analysis**

369 The estimates of avoided direct flood impacts are accounted in a DRR-oriented CBA to evaluate the feasibility
 370 of mitigation measures in terms of NPV, BCR and payback period for the two time-horizons (30 years and 80
 371 years). The assessment does not measure the indirect benefits brought in terms of urban renovation, which are
 372 the primary focus of Parco del Mare project, measuring, instead, only the direct benefits in terms of direct
 373 flood damage reduction. In figure 10, the Expected Annual Benefits (EAB) grow at faster rate approaching
 374 2100 in both sites, because of the larger expected damages from more intense, less frequent flood events. The
 375 cost of defence implementation is repaid by avoided damage after about 40 years in Cesenatico and after 90
 376 years in Rimini. At 2100, the BCR is 0.9 for Rimini and 1.8 for Cesenatico. These results clearly indicate an
 377 overall profitability of the defence structure implementation over the long term for Cesenatico. For the case of
 378 the municipality of Rimini, further investigation is required in order to account for the non-DRR benefits of
 379 the seafront renovation project. For instance, the potential reduction in indirect losses in terms of capital and
 380 labour productivity due to less frequent and less intense flooding events, and the potential increase in tourism
 381 and well-being of citizens due to renewed urban landscape, are factors that could be accounted for in a holistic
 382 CBA analysis and would likely return a shorter payback period.

383 In order to better understand the potential benefits of the mitigation measures over different areas of the two
 384 municipalities, we compare the results in terms of CBR over a selection of exposed records corresponding to
 385 the town higher-density area (i.e. Cesenatico historical center). Table 2 summarizes the metrics of the
 386 assessment for different area extent selections. Results do not differ much when comparing the CBA over
 387 different areas. In Cesenatico benefits grow proportionally to costs, so that the payback time does not change
 388 when considering a section of the town or the whole coastal perimeter.



389

390 **Figure 10.** Cumulated flood defence costs and expected benefits at Net Present Value for Rimini (left) and
 391 Cesenatico (right).
 392

393 **Table 2.** Summary of CBA for planned or designed seaside defence project in Rimini (all town and south
 394 section only) and Cesenatico (all town and center only) over a time horizon of 30 and 80 years (2020 to 2050
 395 and 2020 to 2100).

Metrics	Rimini				Cesenatico			
	All town		South only		All town		Center only	
	2050	2100	2050	2100	2050	2100	2050	2100
Baseline EAD [M EUR]	2.8	32	0.5	14.6	1.7	25.9	0.5	12.4
Defended EAD [M EUR]	2.4	17	0.1	0.9	0.1	0.4	0.1	0.4
Expected Annual Benefits [M EUR]	0.3	15	0.4	13.7	1.6	25.5	0.4	11.9
Sum of EAB (discounted) [M EUR]	5.6	30	4.1	27.8	12.0	79.4	4.7	28.6
Sum of EAC (discounted) [M EUR]	33.8	34.0	33.8	34.0	43.8	44.3	15.8	16.0
Net Present Value [M EUR]	-28.3	-4.0	-29.8	-6.3	-31.8	35.1	-11.24	12.6
Benefit-Cost ratio [-]	0.16	0.88	0.12	0.81	0.28	1.79	0.30	1.79

396 **5. Conclusion**

397 In this study we addressed coastal inundation risk scenarios over two coastal towns located along the North
 398 Adriatic coastal plain of Italy, which is projected to become increasingly exposed to ESL events due to changes
 399 in MSL induced by SLR and subsidence phenomena. Both locations are expected to suffer increasing economic
 400 losses from these events unless effective coastal adaptation measures are put in place. To understand the
 401 upcoming impacts and the potential benefits of designed coastal projects, we run a CBA comparing the
 402 baseline and the defended scenario in terms of flood losses over residential buildings, which represent the
 403 largest share of exposed buildings' footprints (93%). The defended scenario accounts for the effect of a coastal
 404 barriers based on the design of the "Parco del Mare", an urban renovation project under construction in
 405 Rimini. The same type of defence structure is envisaged along the coastal perimeter of the nearby town of
 406 Cesenatico. First, we characterised reference ESL events in terms of frequency and intensity based on local
 407 historical observations; then, we projected ESL scenarios to 2050 and 2100, accounting for the combined effect
 408 of eustatic SLR and subsidence rates on the TWL, as obtained from existing local studies. We produced flood
 409 hazard maps estimating maximum flood extent and water depth using a high-resolution hydrodynamic model
 410 able to replicate the physics of the inundation process. The hazard maps were fed to the damage model in
 411 order to calculate the expected annual damage for both baseline and defended scenarios. An increase in

412 damage is expected for both urban areas from 2020 to 2100: in Cesenatico the EAD grows by a factor 96, in
413 Rimini by a factor 49.

414 The results obtained from the CBA on both locations show growing profitability of present project investment
415 over time, associated with the increase of expected annual damage from intense ESL events: the EAD under
416 the baseline hypothesis is expected to increase by 3.5-fold in 2050, up to 10-fold in 2100. The benefits brought
417 by the coastal defence project become much larger in the second half of the century: the EAB grows 6.1-fold in
418 Rimini, 6.5-fold in Cesenatico, from 2050 to 2100. Avoided losses are expected to match the project
419 implementation costs after about 40 years in Cesenatico and 90 years in Rimini. Benefits are found to increase
420 proportionally to costs; the payback period in Cesenatico is the same considering either an investment on the
421 protection of the whole town or only part of it. Further assessments of these renovation projects should look
422 to measure the indirect and spill-over effects over the local economy brought by the project, possibly
423 accounting also for the intangible benefits and scenarios of exposure change. The results are calculated in
424 relation to emission scenario RCP4.5; compared to RCP8.5 at 2050, the difference in SLR contribution is
425 negligible (~0.05 m), while at 2100, the difference between the two emission scenarios is larger (around 0.2 m),
426 thus additional scenario analysis is suggested in future research.

427 **Data availability**

428 Mattia Amadio, & Arthur H. Essenfelder. (2021). Coastal flood inundation scenarios over Cesenatico and
429 Rimini: hazard and risk for Business as Usual and Defended options [Data set]. *Natural Hazard and Earth*
430 *System Sciences*. <http://doi.org/10.5194/nhess-2020-414>

431 **Authors contribution**

432 MA, AHE and SB conceptualized the study and designed the experiments. AHE carried out the coastal hazard
433 modelling. SR advised the model setup and calculation. SB and PM provided required data and expertise
434 about the case study areas. MA performed the economic risk modelling and wrote the manuscript. SM
435 supported the CBA calculations. JM and SB managed the funding acquisition and project supervision. All co-
436 authors have reviewed the manuscript.

437 **Acknowledgment**

438 The research leading to this paper received funding through the projects CLARA (EU's Horizon 2020 research
439 and innovation programme under grant agreement 730482), SAFERPLACES (Climate-KIC innovation
440 partnership) and EUCP – European Climate Prediction system under grant agreement 776613. We want to
441 thank Luisa Perini for her kind support.

442 **References**

- 443 Amadio M, Scorzini AR, Carisi F, et al (2019) Testing empirical and synthetic flood damage models: the case
444 of Italy. *Nat Hazards Earth Syst Sci* 19:661–678 . doi: 10.5194/nhess-19-661-2019
- 445 Antonioli F, Anzidei M, Amorosi A, et al (2017) Sea-level rise and potential drowning of the Italian coastal
446 plains: Flooding risk scenarios for 2100. *Quat Sci Rev* 158:29–43 . doi: 10.1016/j.quascirev.2016.12.021
- 447 Armaroli C, Ciavola P, Perini L, et al (2012) Critical storm thresholds for significant morphological changes
448 and damage along the Emilia-Romagna coastline, Italy. *Geomorphology* 143–144:34–51 . doi:
449 10.1016/j.geomorph.2011.09.006

- 450 Armaroli C, Duo E (2018) Validation of the coastal storm risk assessment framework along the Emilia-
451 Romagna coast. *Coast Eng* 134:159–167 . doi: 10.1016/j.coastaleng.2017.08.014
- 452 Boardman AE, Greenberg DH, Vining AR, Weimer DL (2018) *Cost-Benefit Analysis*. Cambridge University
453 Press
- 454 Bonaduce A, Pinardi N, Oddo P, et al (2016) Sea-level variability in the Mediterranean Sea from altimetry
455 and tide gauges. *Clim Dyn* 47:2851–2866 . doi: 10.1007/s00382-016-3001-2
- 456 Bos F, Zwaneveld P (2017) *Cost-Benefit Analysis for Flood Risk Management and Water Governance in the*
457 *Netherlands: An Overview of One Century*. SSRN Electron J. doi: 10.2139/ssrn.3023983
- 458 Bouwer LM (2011) Have disaster losses increased due to anthropogenic climate change? *Bull Am Meteorol*
459 *Soc*. doi: 10.1175/2010BAMS3092.1
- 460 Carbognin L, Teatini P, Tomasin A, Tosi L (2010) Global change and relative sea level rise at Venice: What
461 impact in term of flooding. *Clim Dyn* 35:1055–1063 . doi: 10.1007/s00382-009-0617-5
- 462 Carbognin L, Teatini P, Tosi L (2009) The impact of relative sea level rise on the Northern Adriatic Sea coast,
463 Italy. *WIT Trans Ecol Environ* 127:137–148 . doi: 10.2495/RAV090121
- 464 Carminati E, Martinelli G (2002) Subsidence rates in the Po Plain, northern Italy: the relative impact of
465 natural and anthropogenic causation. *Eng Geol* 66:241–255 . doi: 10.1016/S0013-7952(02)00031-5
- 466 Church JA, White NJ (2011) Sea-Level Rise from the Late 19th to the Early 21st Century. *Surv Geophys*
467 32:585–602 . doi: 10.1007/s10712-011-9119-1
- 468 Ciavola P, Coco G (eds) (2017) *Coastal storms: processes and impacts*. Wiley-Blackwell
- 469 Comune di Rimini (2018) *Parco del Mare Sud - Strategia per la rigenerazione urbana*
- 470 Comune di Rimini (2019a) *Deliberazione originale di giunta comunale N. 99 del 11/04/2019*
- 471 Comune di Rimini (2019b) *Deliberazione originale di giunta comunale N. 118 del 02/05/2019*
- 472 Comune di Rimini (2020) *Deliberazione originale di giunta comunale N. 128 del 26/05/2020*
- 473 Comune di Rimini (2021a) *Deliberazione originale di giunta comunale N. 19 del 19/01/2021*
- 474 Comune di Rimini (2021b) *Deliberazione originale di giunta comunale N. 20 del 19/01/2021*
- 475 CRESME (2014) *Definizione dei costi di (ri)costruzione nell’edilizia*
- 476 Froehlich DC (2002) *IMPACT Project Field Tests 1 and 2: “Blind” Simulation*. 1–18
- 477 Gambolati G, Giunta G, Putti M, et al (1998) Coastal Evolution of the Upper Adriatic Sea due to Sea Level
478 Rise and Natural and Anthropic Land Subsidence. 1–34 . doi: 10.1007/978-94-011-5147-4
- 479 Garnier E, Ciavola P, Spencer T, et al (2018) Historical analysis of storm events: Case studies in France,
480 England, Portugal and Italy. *Coast Eng* 134:10–23 . doi: 10.1016/j.coastaleng.2017.06.014
- 481 Geofabrik GmbH (2018) *OpenStreetMap data extracts*
- 482 Hallegatte S, Green C, Nicholls RJ, Corfee-Morlot J (2013) Future flood losses in major coastal cities. *Nat*
483 *Clim Chang*. doi: 10.1038/nclimate1979
- 484 Hinkel J, Lincke D, Vafeidis AT, et al (2014) Coastal flood damage and adaptation costs under 21st century
485 sea-level rise. *Proc Natl Acad Sci*. doi: 10.1073/pnas.1222469111
- 486 Huizinga J, Moel H De, Szewczyk W (2017) *Global flood depth-damage functions : Methodology and the*
487 *Database with Guidelines*
- 488 IPCC (2019) *IPCC Special Report on the Ocean and Cryosphere in a Changing Climate*
- 489 ISPRA (2012) *Mare e ambiente costiero. Temat Primo Piano - Annu dei dati Ambient 2011 259–322*

- 490 ISTAT (2011) 15° censimento della popolazione e delle abitazioni
- 491 Jongman B, Kreibich H, Apel H, et al (2012a) Comparative flood damage model assessment: towards a
492 European approach. *Nat Hazards Earth Syst Sci* 12:3733–3752
- 493 Jongman B, Ward PJ, Aerts JCJH (2012b) Global exposure to river and coastal flooding: Long term trends
494 and changes. *Glob Environ Chang*. doi: 10.1016/j.gloenvcha.2012.07.004
- 495 Jonkman SN, Brinkhuis-Jak M, Kok M (2004) Cost benefit analysis and flood damage mitigation in the
496 Netherlands. *Heron* 49:95–111
- 497 Kain CL, Lewarn B, Rigby EH, Mazengarb C (2020) Tsunami Inundation and Maritime Hazard Modelling
498 for a Maximum Credible Tsunami Scenario in Southeast Tasmania, Australia. *Pure Appl Geophys*
499 177:1549–1568 . doi: 10.1007/s00024-019-02384-0
- 500 Kemp AC, Horton BP, Donnelly JP, et al (2011) Climate related sea-level variations over the past two
501 millennia. *Proc Natl Acad Sci U S A* 108:11017–11022 . doi: 10.1073/pnas.1015619108
- 502 Kind JM (2014) Economically efficient flood protection standards for the Netherlands. *J Flood Risk Manag*
503 7:103–117 . doi: 10.1111/jfr3.12026
- 504 Kirezci E, Young IR, Ranasinghe R, et al (2020) Projections of global-scale extreme sea levels and resulting
505 episodic coastal flooding over the 21st Century. *Sci Rep* 10:1–12 . doi: 10.1038/s41598-020-67736-6
- 506 Lambeck K, Antonioli F, Anzidei M, et al (2011) Sea level change along the Italian coast during the Holocene
507 and projections for the future. *Quat Int* 232:250–257 . doi: 10.1016/j.quaint.2010.04.026
- 508 Lambeck K, Purcell A (2005) Sea-level change in the Mediterranean Sea since the LGM: Model predictions
509 for tectonically stable areas. In: *Quaternary Science Reviews*. Pergamon, pp 1969–1988
- 510 Lionello P (2012) The climate of the Venetian and North Adriatic region: Variability, trends and future
511 change. *Phys Chem Earth* 40–41:1–8 . doi: 10.1016/j.pce.2012.02.002
- 512 Lionello P, Barriopedro D, Ferrarin C, et al (2020) Extremes floods of Venice: characteristics, dynamics, past
513 and future evolution. *Nat Hazards Earth Syst Sci* 1–34 . doi: 10.5194/nhess-2020-359
- 514 Lowe J (2008) Intergenerational wealth transfers and social discounting: Supplementary Green Book
515 guidance. HM Treasury, London 3–6
- 516 Lowe J, Gregory J, Flather R (2001) Changes in the occurrence of storm surges around the United Kingdom
517 under a future climate scenario using a dynamic storm surge model driven by the Hadley Centre
518 climate models. *Clim Dyn* 18:179–188
- 519 Marsico A, Lisco S, Lo Presti V, et al (2017) Flooding scenario for four Italian coastal plains using three
520 relative sea level rise models. *J Maps* 13:961–967 . doi: 10.1080/17445647.2017.1415989
- 521 Masina M, Lamberti A, Archetti R (2015) Coastal flooding: A copula based approach for estimating the joint
522 probability of water levels and waves. *Coast Eng* 97:37–52 . doi: 10.1016/j.coastaleng.2014.12.010
- 523 McGranahan G, Balk D, Anderson B (2007) The rising tide: Assessing the risks of climate change and human
524 settlements in low elevation coastal zones. *Environ Urban*. doi: 10.1177/0956247807076960
- 525 McInnes KL, Walsh KJE, Hubbert GD, Beer T (2003) Impact of sea-level rise and storm surges in a coastal
526 community. *Nat Hazards* 30:187–207 . doi: 10.1023/A:1026118417752
- 527 Mechler R (2016) Reviewing estimates of the economic efficiency of disaster risk management: opportunities
528 and limitations of using risk-based cost–benefit analysis. *Nat Hazards* 81:2121–2147 . doi:
529 10.1007/s11069-016-2170-y
- 530 Meli M, Olivieri M, Romagnoli C (2021) Sea-level change along the emilia-romagna coast from tide gauge
531 and satellite altimetry. *Remote Sens* 13:1–26 . doi: 10.3390/rs13010097
- 532 Meyssignac B, Cazenave A (2012) Sea level: A review of present-day and recent-past changes and variability.

- 533 J. Geodyn. 58:96–109
- 534 Mitchum GT, Nerem RS, Merrifield MA, Gehrels WR (2010) Modern Sea-Level-Change Estimates. In:
535 Understanding Sea-Level Rise and Variability. Wiley-Blackwell, Oxford, UK, pp 122–142
- 536 Muis S, Verlaan M, Winsemius HC, et al (2016) A global reanalysis of storm surges and extreme sea levels.
537 Nat Commun 7:1–11 . doi: 10.1038/ncomms11969
- 538 Nicholls RJ, Cazenave A (2010) Sea-level rise and its impact on coastal zones. Science (80-) 328:1517–1520 .
539 doi: 10.1126/science.1185782
- 540 Olsen AS, Zhou Q, Linde JJ, Arnbjerg-Nielsen K (2015) Comparing methods of calculating expected annual
541 damage in urban pluvial flood risk assessments. Water (Switzerland) 7:255–270 . doi: 10.3390/w7010255
- 542 Peltier WR (2004) Global Glacial Isostasy and the surface of the ice-age Earth: the ICE-5G (VM2) Model and
543 GRACE. Annu Rev Earth Planet Sci 32:111–149 . doi: 10.1146/annurev.earth.32.082503.144359
- 544 Peltier WR, Argus DF, Drummond R (2015) Space geodesy constrains ice age terminal deglaciation: The
545 global ICE-6G_C (VM5a) model. J Geophys Res Solid Earth 120:450–487 . doi: 10.1002/2014JB011176
- 546 Perini L, Calabrese L, Deserti M, et al (2011) Le mareggiate e gli impatti sulla costa in Emilia-Romagna 1946-
547 2010
- 548 Perini L, Calabrese L, Lorito S, Luciani P (2015) Il rischio da mareggiata in Emilia-Romagna: l’evento del 5-6
549 Febbraio 2015. Geol 53:8–17
- 550 Perini L, Calabrese L, Luciani P, et al (2017) Sea-level rise along the Emilia-Romagna coast (Northern Italy) in
551 2100: Scenarios and impacts. Nat Hazards Earth Syst Sci 17:2271–2287 . doi: 10.5194/nhess-17-2271-2017
- 552 Perini L, Calabrese L, Salerno G, Luciani P (2012) Mapping of flood risk in Emilia-Romagna coastal areas.
553 Rend Online Soc Geol Ital 21:501–502 . doi: 10.13140/2.1.1703.7766
- 554 Polcari M, Albano M, Montuori A, et al (2018) InSAR monitoring of Italian coastline revealing natural and
555 anthropogenic ground deformation phenomena and future perspectives. Sustain 10:4–7 . doi:
556 10.3390/su10093152
- 557 Price R (2018) Cost-effectiveness of disaster risk reduction and adaptation to climate change. 1–21
- 558 Roberts S (2020) ANUGA - Open source hydrodynamic / hydraulic modelling
- 559 Roberts S, Nielsen O, Gray D, Sexton J (2015) ANUGA User Manual
- 560 Solari L, Del Soldato M, Bianchini S, et al (2018) From ERS 1/2 to Sentinel-1: Subsidence Monitoring in Italy
561 in the Last Two Decades. Front Earth Sci 6: . doi: 10.3389/feart.2018.00149
- 562 Stocker TF, Dahe Q, Plattner G-K, et al (2013) Technical Summary. In: Stocker TF, Qin D, Plattner G-K, et al.
563 (eds) Climate Change 2013: The Physical Science Basis. Contribution of Working Group I to the Fifth
564 Assessment Report of the Intergovernmental Panel on Climate Change. Cambridge University Press,
565 Cambridge, United Kingdom and New York, NY, USA., pp 33–115
- 566 Syvitski JPM, Kettner AJ, Overeem I, et al (2009) Sinking deltas due to human activities. Nat Geosci. doi:
567 10.1038/ngeo629
- 568 Teatini P, Ferronato M, Gambolati G, Gonella M (2006) Groundwater pumping and land subsidence in the
569 Emilia-Romagna coastland, Italy: Modeling the past occurrence and the future trend. Water Resour Res
570 42: . doi: 10.1029/2005WR004242
- 571 Tsimplis MN, Raicich F, Fenoglio-Marc L, et al (2012) Recent developments in understanding sea level rise at
572 the Adriatic coasts. Phys Chem Earth 40–41:59–71 . doi: 10.1016/j.pce.2009.11.007
- 573 Tsimplis MN, Rixen M (2002) Sea level in the Mediterranean Sea: The contribution of temperature and
574 salinity changes. Geophys Res Lett 29:51-1-51–4 . doi: 10.1029/2002gl015870
- 575 Umgiesser G, Bajo M, Ferrarin C, et al (2020) The prediction of floods in Venice: methods, models and

576 uncertainty. Nat Hazards Earth Syst Sci 1–47 . doi: 10.5194/nhess-2020-361

577 Vousdoukas MI, Mentaschi L, Feyen L, Voukouvalas E (2017) Extreme sea levels on the rise along Europe’s

578 coasts. Earth’s Futur 5:1–20 . doi: 10.1002/ef2.192

579 Vousdoukas MI, Mentaschi L, Voukouvalas E, et al (2018) Global probabilistic projections of extreme sea

580 levels show intensification of coastal flood hazard. Nat Commun 9:1–12 . doi: 10.1038/s41467-018-

581 04692-w

582 Wöppelmann G, Marcos M (2012) Coastal sea level rise in southern Europe and the nonclimate contribution

583 of vertical land motion. J Geophys Res Ocean 117: . doi: 10.1029/2011JC007469

584 Zanchettin D, Bruni S, Raicich F, et al (2020) Review article: Sea-level rise in Venice: historic and future

585 trends. Nat Hazards Earth Syst Sci Discuss 1–56 . doi: 10.5194/nhess-2020-351

586 Zanchettin D, Traverso P, Tomasino M (2007) Observations on future sea level changes in the Venice lagoon.

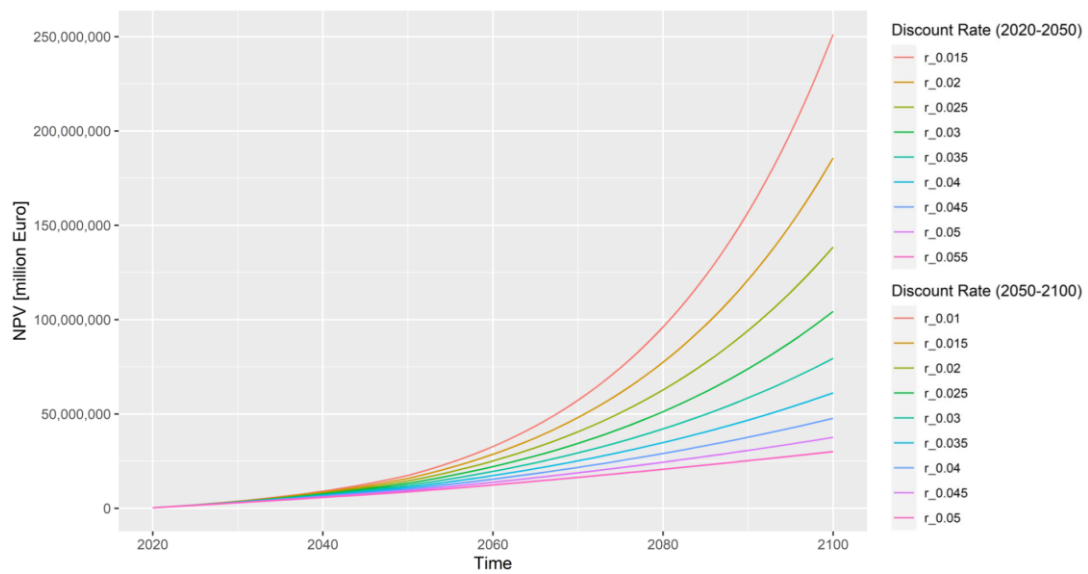
587 Hydrobiologia. doi: 10.1007/s10750-006-0416-5

588

589 **Annex 1**

590 A sensitivity analysis is carried out on the discount rate. Figure A1 below shows how the NPV changes with

591 discount rate r ranging from 1.5% to 5.5% (2020 to 2050) and 1% to 5% (2050-2100).



592

593 **Figure A1.** Sensitivity analysis of NPV using a variable discount rate.